LA-UR-16-28621
Approved for public release; distribution is unlimited.

Title: Characterization of the Geosynchronous Plasma Environment for the SENSER/RROE Optical Instrument

Author(s): Woodroffe, Jesse Richard

Intended for: Report

Issued: 2016-11-08

Characterization of the Geosynchronous Plasma Environment For the SENSER/RROE Optical Instrument

Jesse Woodroffe
ISR-1: Space Science & Applications
Los Alamos National Laboratory

Summary

In this report, we summarize available research in order to characterize expected rates of particle incidence on the SENSER/RROE optical instrument. We first investigate the "normal" background levels using data from statistical studies of spacecraft in geosynchronous orbit and empirical models. We then consider "worst case" scenarios based on event studies in which extreme fluxes have been observed. We use these data to define "maximum" rates of particle incidence. We then consider how incident particles will actually produce counts in the instrument by considering the effects of screening by the instrument housing and the possibility of direct particle access to the housing, with rates for both primary access and secondary electron generation.

I. Climatology of Geosynchronous Particle Fluxes

A. Statistical Background Characterization from LANL GEO Data

The average geosynchronous plasma environment is a well-characterized environment, thanks in no small part to an extensive database of measurements from the LANL GEO spacecraft. For example, *Thomsen et al.* [2007] used more than 10 years of data to obtain a detailed statistical characterization of geosynchronous particle fluxes for particle energies between 40 eV and 45 keV, the results of which are shown in **Figure 1**. At higher energies, *O'Brien et al.* [2007] studied the fluxes of electrons with energies up to 4.7 MeV. (It is important to note that the data expressed in **Figures 1-2** are in different units; for quantitative comparison, the data from **Figure 1** should be multiplied by 10^3.)

According to the data from *Thomsen et al.*, electron fluxes (at or above median level) decrease monotonically with energy while ion fluxes (similarly at or above median level) have a localized peak in fluxes just above 10 eV. The monotonic decrease in electron fluxes continues in the data set presented by *O'Brien et al.*, with fluxes at 1 MeV approximately 10^{-3} lower than fluxes at 100 keV. The highest electron and proton fluxes (j_e and j_p , respectively) in **Figure 1** are $j_e \approx 3\times10^{11}$ cm^{-2} sr^{-1} s^{-1}keV^{-1} and $j_p \approx 5\times10^{9}$ cm^{-2} sr^{-1} s^{-1}keV^{-1}. As can be seen in **Figure 1**, the median background levels are at least order of magnitude (~10-50x) smaller than these enhancements, $j_{e,med} \approx 1.5\times10^{10}$ cm^{-2} sr^{-1} s^{-1}keV^{-1} and $j_{p,med} \approx 1.5\times10^{7}$ cm^{-2} sr^{-1} s^{-1}keV^{-1}.

B. Quantitative Background Prediction with AE9/AP9 Models

An alternative to single-source statistical characterization is multi-source parameterized models such as the AE9/AP9 empirical flux model [*Ginet et al.*, 2013]. These models allow us to "fly" a virtual satellite for an extended period of time, determining instantaneous particle fluxes at specified energies and times for the duration of the simulation. Natural variability is accounted for in these models by using a Monte Carlo approach to pick values from a distribution of flux profiles; by running multiple simulations, we are able to build a distribution of fluxes that can then be used to provide percentile measurements.

The results from a one-year simulation of a geostationary spacecraft are shown in **Figure 3**. We have calculated the fluxes along a geostationary orbit using 40 different AE9/AP9 runs. The results from each of these runs were aggregated in order to determine the 95th percentile level fluxes for a variety of different energies. Kernel density estimation was used to obtain an empirical probability distribution for flux levels based on the entire year of data for each of the particle energies we modeled. Using the kernel density estimators, we were then able to determine 90% confidence intervals (CIs) for the 95% flux levels. The net result of this analysis was a well-defined range of possibilities for a reasonable "worst case" background levels. (It should be noted that our results are in yet another different set of units, with comparison to **Figure 2** requiring multiplication by 10^{-3}; this multiplication has been applied for the values quoted below. In addition, the fluxes in both *Thomsen et al.* and *O'Brien et al.* are given per unit of solid angle, so there may be an additional factor of up to 4π required to reconcile these values.)

How large are the background fluxes predicted by the AE9/AP9 models? For both electrons and protons, the peak fluxes occur at lower energies, with $j_e > 10^7 \mathrm{cm}^{-2}\mathrm{s}^{-1}\mathrm{keV}^{-1}$ for energies up to 100 keV and $j_e > 10^4 \mathrm{cm}^{-2}\mathrm{s}^{-1}\mathrm{keV}^{-1}$ for energies up to 1 MeV. For protons, the background fluxes are smaller by an order of magnitude or more ($j_e/j_p \approx \sqrt{m_i/m_e}$, where m_i/m_e is the proton to electron mass ratio), with $j_p \approx 10^5 \mathrm{cm}^{-2}\mathrm{s}^{-1}\mathrm{keV}^{-1}$ at 100 keV energies and $j_p \approx 10\ \mathrm{cm}^{-2}\mathrm{s}^{-1}\mathrm{keV}^{-1}$ at 1 MeV.

C. Cosmic Rays

Cosmic rays are fully ionized highly energetic atomic nuclei (electrons are also present, but their fluxes are two orders of magnitude lower). There are two primary populations of cosmic rays in the Earth's magnetosphere – solar energetic particles (SEPs) and galactic cosmic rays (GCRs). The occurrence of SEPs is strongly linked to solar activity, and the resultant flux of charged particle radiation may vary by orders of magnitude between events. We will discuss some worst-case SEP events in Section II.A.

Unlike SEPs, the GCR background is both omnipresent and (to much greater degree) isotropic. The composition of GCRs is almost entirely light elements, with the primary constituents being Hydrogen (90%) and Helium (9%). The GCR background has well-known solar cycle dependence [*Parker*, 1958], with fluxes decreasing with increasing levels of solar activity. Consequently, the GCR background is strongest during solar minimum. *Zetlin et al.* [2016] used measurements from the CRaTER instrument on the Lunar Reconnaissance Orbiter to measure the variation of GCR fluxes during the 2009-2014 transition from solar minimum to solar maximum (**Figure 4**). This particular cycle was historically weak, with a deep minimum in late 2009 and a very weak maximum in 2014. Based on our understanding of GCR flux modulation, this suggests that observed fluxes of GCRs are unlikely to be much worse than those in late 2009 (**Figure 5**). According to *Zetlin et al.*, standard models such as CREME [*Tylka et al.*, 1997] and DLR [*Matthiä et al.*, 2013] have been found to underestimate fluxes by as much as 25% for this period.

Based on **Figure 5**, we can estimate that **GCR (>180 MeV) counts are typically around 240 per 10 minutes (0.4 s^{-1}), and they will only rarely exceed 400 per 10 minutes (0.667 s^{-1})**. The knock-on and cascade effects of GCR impact are beyond the scope of this document.

II. Historical Worst Cases

The climatological data from the previous section does incorporate the effects of geomagnetic activity, but due to the statistical methods applied to their analysis, the "worst" case climatological

prediction typically far undershoots the actual observed worst cases. In this section, we will review single event worst-case scenarios produced by geomagnetic storms and related solar activity.

A. Storm-time Geosynchronous Flux Enhancements

In late July 2004, a series of four coronal mass ejections (CMEs) were ejected earthward over the course of seven days. This lead to a unique geomagnetic storm of extended duration, during which time the GOES spacecraft observed the largest-ever fluxes of >2 MeV electrons in the entire history of their mission. According to *Meredith et al.* [2015], **daily-average integral fluxes peaked at 4.92×10^5 cm^{-2}sr^{-1}s^{-1} on July 29, 2004, and fluxes were above 1.0×10^5 cm^{-2}sr^{-1}s^{-1} for nearly a week surrounding this day.**

B. Solar Energetic Particle Events

In late October through early November 2003, a series of CMEs were launched earthward from the sun, ultimately resulting in one of the strongest geomagnetic storms since the advent of the space age. This "Halloween" storm as it has come to be called, was also accompanied by an incredibly strong enhancement of energetic charged particles, an occurrence known as a solar energetic particle (SEP) event. *Mewaldt et al.* [2005] performed a case study of significant SEP events, including the Halloween storm, finding that it was highly similar to other extreme events, and should therefore be useful as a representative "worst case" event (see **Figure 6**).

The Halloween SEP event reached 29500 pfu[1], making it the fourth strongest SEP event in NOAA's database (ftp://ftp.swpc.noaa.gov/pub/indices/SPE.txt), with fluxes within a factor of two or so of the largest ever observed. **Between 11 UT on 28 October 2003 and 20 UT on 29 October 2003, the average *E*>40 MeV proton flux as measured by the geosynchronous spacecraft exceeded 6.5×10^6 cm^{-2}sr^{-1}s^{-1}.** It is almost certain that the peak fluxes far exceeded this average level at some point during this storm. Proton fluxes at lower energies were also enhanced, with the entire spectrum being well represented by a broken power law; even larger fluxes of protons with energies $1 \leq E < 40$ MeV also were observed.

An alternative quantitative source for extreme solar proton fluxes is the CREME-96 solar proton model [*Tylka et al.*, 1997]. **Figure 7** shows the "5 minute peak" solar proton event spectrum obtained from CREME-96. Integration of this spectrum for energies above 40 MeV yields a result that is within a factor a few of *Mewaldt et al.*'s numbers for the Halloween storm. Perhaps more interesting, however, is the sharp increase in fluxes at lower energies, with >1 MeV proton fluxes exceeding 10^8 cm^{-2}s^{-1}sr^{-1}.

III. Predicted Rates of Single Particle Incidence

There are two main ways in which a particle can reach the detector. First, it can penetrate the enclosure of the instrument and directly impact the detector. Second, a particle can enter through the aperture and impact the interior of the housing; this impact results in the generation of some multiplicity of secondary particles that then propagate to the detector. We will limit our consideration here to only penetrating particles.

[1] Proton flux unit. 1 pfu = 1 cm^{-2}sr^{-1}s^{-1} for energies above 10 MeV. Note that this is slightly different than the pfu used in **Figure 4**, which was for energies above 180 MeV.

A. Penetration Depths

The enclosure of SENSER is composed of 3/8" (9.525 mm) Aluminum (Z=13). This material presents a significant barrier for incident charged particles. According to the NIST ESTAR and PSTAR programs (http://www.nist.gov/pml/data/star/index.cfm), collisions are the primary stopping mechanism for particles incident on Aluminum at the energies of interest to the current study. As **Figure 8** shows, the stopping power is strongly dependent on incident particle energy, with electron stopping power minimizing near an MeV and proton stopping power minimizing at a few GeV. However, because of the thickness of the enclosure, it is necessary to consider not just the stopping power at the surface but also the depth to which an incident particle can penetrate.

Using the stopping power data from **Figure 8**, we can determine the depth through which an energetic particle can penetrate the SENSER enclosure. By integrating the particle trajectory through the aluminum enclosure and assuming a continuous loss of energy due to collisions (the continuous slowing down approximation, or CSDA), we find that electrons should have energies of at least 4.625 MeV to penetrate the enclosure, while protons (which are much more strongly affected by collisions) should have an energies of at least 46.8 MeV.

B. Penetrating Charged Particle Fluxes

Even during worst-case geomagnetic events, the flux of electrons with energies above 4 MeV is typically quite low. Consequently, it is not necessary to worry about electron penetration of the housing. However, as noted in the previous section, significant fluxes of protons with energies above 40 MeV are known to occur in some rare cases.

Using an integrated proton flux of 6.5×10^{6} $cm^{-2}sr^{-1}s^{-1}$, we can estimate the maximum total rate of particle incidence on the detector. Since SEP events are of solar origin by definition, it would be expected that at most 2π sr is exposed to the SEP source (the entire sunward facing half). Using an integrated proton flux of 6.5×10^{6} $cm^{-2}sr^{-1}s^{-1}$, we find a penetrating proton flux of $\approx 4.0\times10^{7}$ $cm^{-2}s^{-1}$. For a sensor with dimensions 1.4 mm by 1.4 mm, we have maximum exposed area of 0.02 cm^2. **Thus, we estimate the worst-case SEP proton count rate of $\approx 8\times10^{5}$ s^{-1}.**

III. Conclusions

Using a combination of statistical data and numerical models, we have characterized the geosynchronous plasma environment and determined the worst-case particle fluxes that could be observed by spacecraft carrying the SENSER/RROE optical instrument. We have found that owing to the thickness of the aluminum enclosure, it is highly unlikely that the natural trapped particle background will be able to cause any significant contamination of the sensor. The drastic increase in energetic protons during an SEP event represents that "worst case" for noise due to direct particle intrusion through the detector housing. Although we did not consider the generation and incidence of secondary particles in any detail, a cursory examination of the literature [*Lin & Joy*, 2005; *Svensson & Holme*n, 1981] suggests that this could be an important effect for typical particle energies at geosynchronous orbit (shown in **Figure 1**). This would be best addressed using a specialized transport code (such as GEANT or MCNP) along with a detailed model of the housing and its interior structure.

References

Ginet, G. P., T. P. O'Brien, S. L. Huston, W. R. Johnson, T. B. Guild, R. Friedel, C. D. Lindstrom, C. J. Roth, P. Whelan, R. A. Quinn, D. Madden, S. Morley, and Y.-J. Su (2013), AE9, AP9 and SPM: New models for specifying the trapped energetic particle and space plasma environment, *Spa. Sci. Rev*., 179(1):579-615, doi:10.1007/s11214-013-9964-y

Lin, Y. and Joy, D. C. (2005), A new examination of secondary electron yield data. *Surf. Interface Anal.*, 37: 895–900. doi:10.1002/sia.2107

Matthiä, D., T. Berger, A. I. Mrigakshi, and G. Reitz (2013), A ready to use galactic cosmic ray model, *Adv. Spa. Res.*, 51(3), 329-338, doi:10.1015/j.asr.2012.09.022

Mewaldt, R. A., C. M. S. Cohen, A. W. Labrador, R. A. Leake, G. M. Mason, M. I. Desai, M. D. Looper, J. E. Mazur, R. S. Selesnik, and D. K. Haggerty (2005), Proton, Helium, and electron spectra during the large solar particle events of October-November 2003*, J. Geophys. Res.*, 110(A09S18), doi:10.1029/2005JA011038

Meredith, N. P., R. B. Horne, J. D. Isle, and J. V. Rodriguez (2015), Extreme relativistic electron fluxes at geosynchronous orbit: Analysis of GOES > 2 MeV electrons, *Spa. Weath.*, 13:170-184, doi:10.1002/2014SW00143

Miroshnichenko, L. I. and R. A. Nymmik (2014), Extreme fluxes in solar energetic particle events: Methodological and physical limitations, *Rad. Meas.*, 61:6-15, doi:10.1016/j.radmeas.2013.11.010

O'Brien, T. P., J. F. Fennell, J. L. Roeder, and G. D. Reeves (2007), Extreme electron fluxes in the outer zone, *Spa. Weath*., 5(S01001), doi:10.1029/2006SW000240

Parker, E. N. (1958), Cosmic-ray modulation by solar wind, Phys. Rev. Lett., 110(6):1445-1449, doi: 10.1103/PhysRev.110.1445

Svensson, B. and G. Holmen (1981), Electron emission from ion-bombarded aluminum, *J. Appl. Phys.*, 52:6928-6933, doi:10.1063/1.328646

Thomsen, M. F., M. H. Denton, B. Lavraud, and M. Bodeau (2007), Statistics of plasma fluxes at geosynchronous orbit over more than a full solar cycle, *Spa. Weath*., 5(S03004), doi:10.1029/2006SW000257

Tylka, A. J., J. H. Adams, P. R. Boberg, B. Brownstein, W. F. Dietrich, E. O. Flueckiger, E. L. Petersen, M. A. Shea, D. F. Smart, E. C. Smith (1997), CREME96: A Revision of the Cosmic Ray Effects on Micro-Electronics Code, *IEEE Trans. Nuc. Sci.*, 44(6):2150-2160, doi:10.1109/23.659030

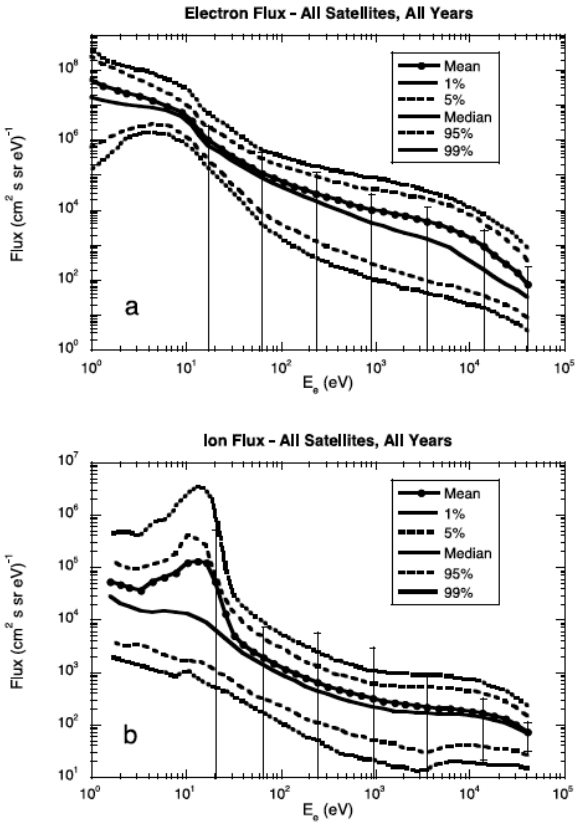

Figure 1. Statistics of geosynchronous electron fluxes from LANL GEO spacecraft [Thomsen et al., 2007].

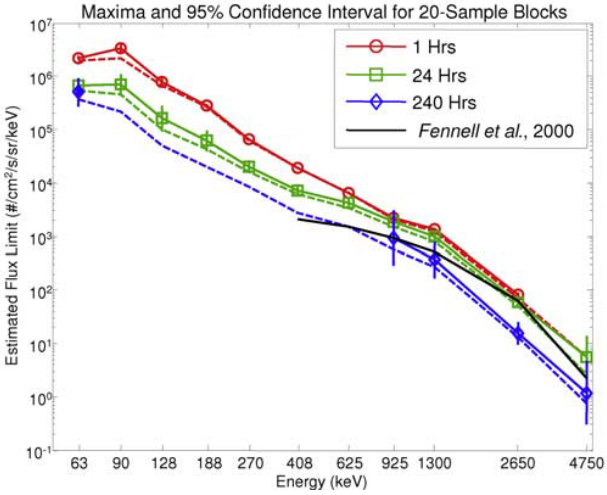

Figure 2. Extreme geosynchronous electron flux levels [*O'Brien et al.*, 2007].

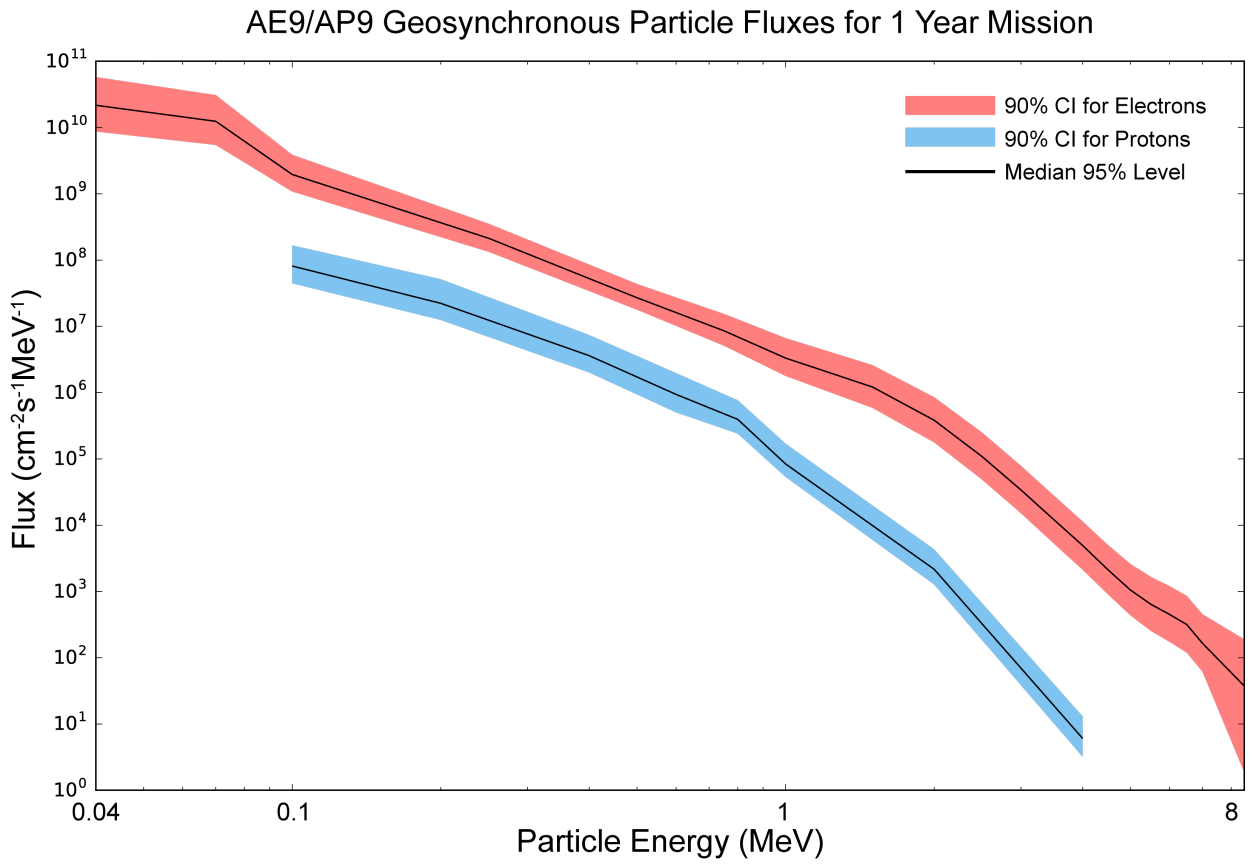

Figure 3. Particle fluxes at 95% level calculated using AE9/AP9 model for a spacecraft in geosynchronous orbit. The colored bands show 90% confidence intervals (CI) on the flux values, with the median for each particle type plotted in black.

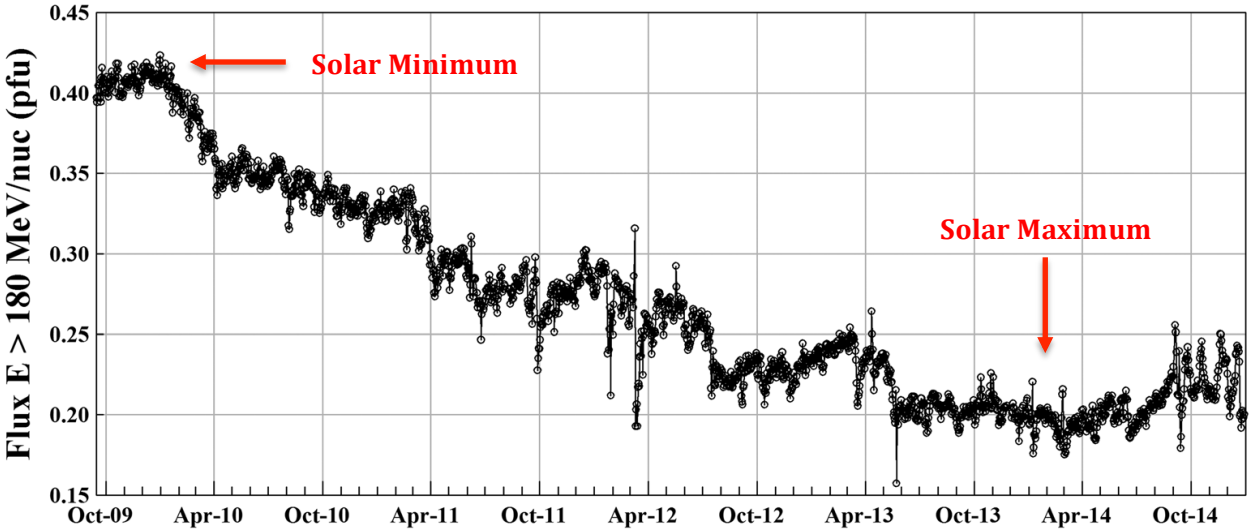

Figure 4. Galactic cosmic ray proton fluxes for energies above 180 MeV measured by the CRaTER instrument aboard Lunar Reconnaissance Orbiter [modified from Figure 4 of *Zeitlin et al.*, 2016]. The units of the y-axis are particle flux units (pfu), where 1 pfu = particles $cm^{-2}sr^{-1}s^{-1}$.

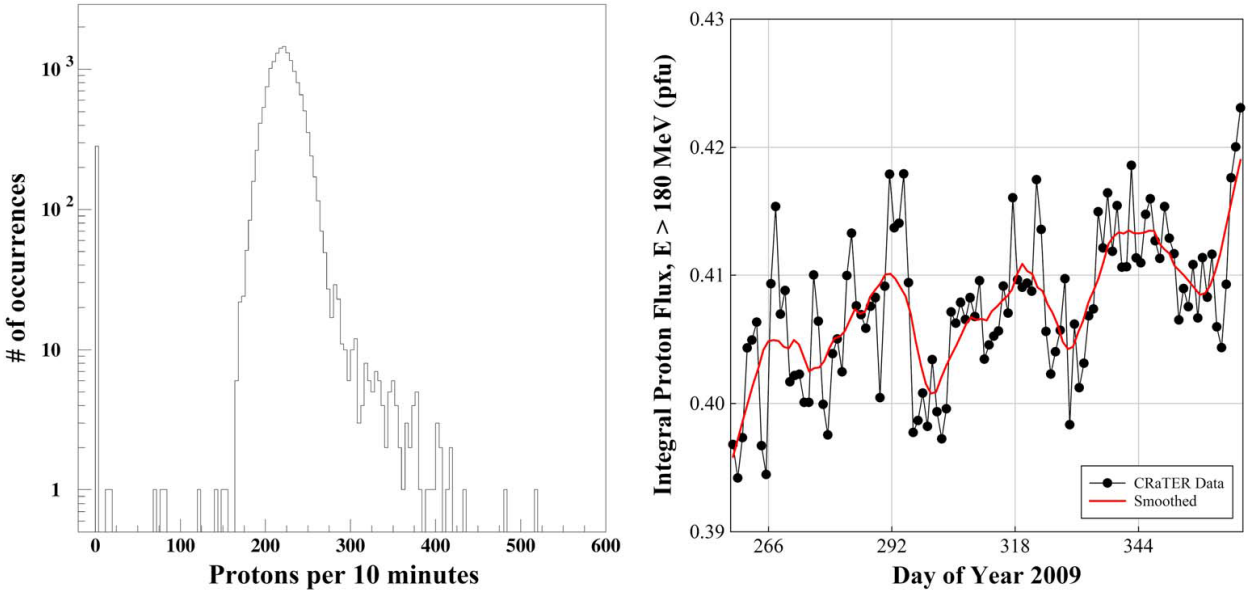

Figure 5. Proton counts (E>180 MeV) from the CRaTER instrument from late 2009 (a period of peak GCR flux).

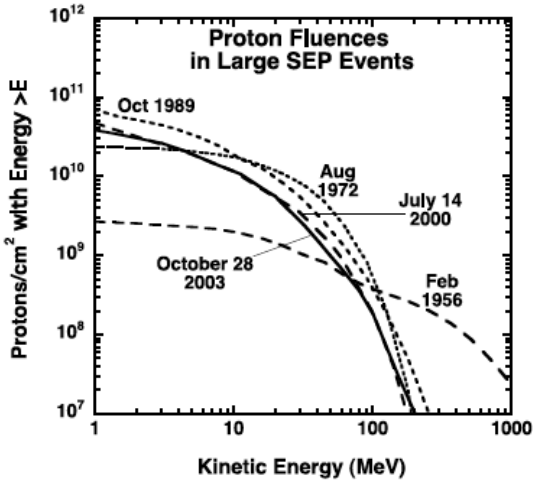

Figure 6. Proton fluence spectra from the largest historical SEP events. The "Halloween" storm is plotted with a solid black line [*Mewaldt et al.*, 2005].

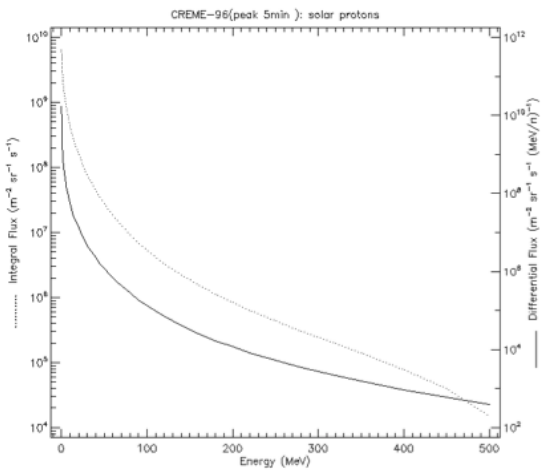

Figure 7. Estimated five-minute "worst case" solar proton fluxes from the CREME-96 model [*Tylka et al.*, 1997], data provided by SPENVIS.

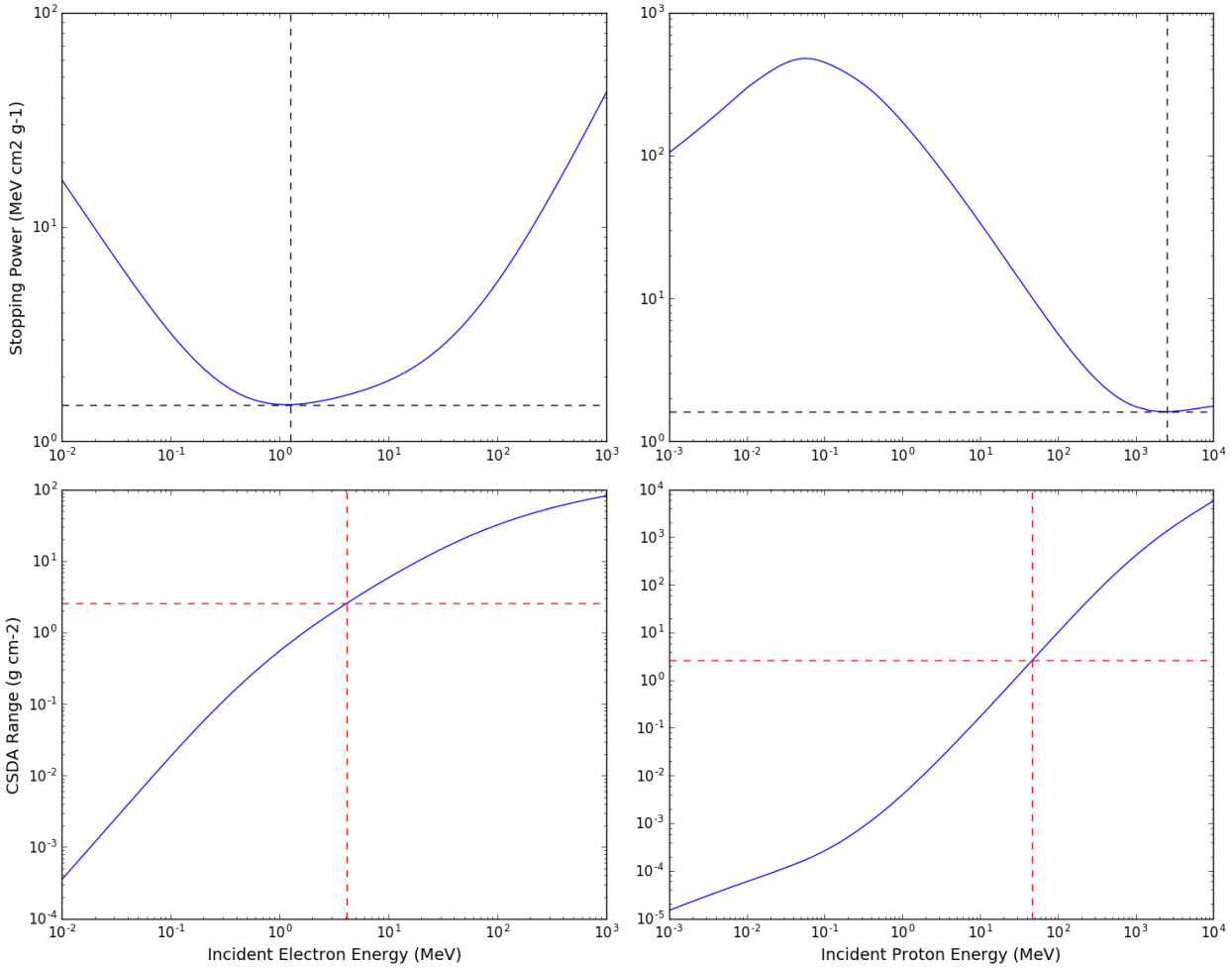

Figure 8. Stopping power and Penetration ranges in the continuous slowing-down approximation (CSDA) obtained from the NIST ESTAR and PSTAR programs. In the top two panels, the dashed black lines locate the minimum stopping power; in the bottom two panels, the dashed red lines locate the energies where penetration through 3/8" Al is expected (4.625 MeV for electrons, 46.8 MeV for protons).